International Journal of Heat and Technology
Vol. 42, No. 5, October, 2024, pp. 1605-1612
Journal homepage: http://iieta.org/journals/ijht

A Numerical Analysis of Cylindrical and Conical Pin Fins Configurations for Enhancing Heat Exchanger Performance

Ali M. Mohsen[1*], Ali M. Tukkee[2], Teh Aun Yao[3]

[1] College of Engineering, University of Warith Al-Anbiyaa, Karbala 56001, Iraq
[2] Department of Petroleum Engineering, University of Kerbala, Karbala 56001, Iraq
[3] School of Engineering, Taylor's University, Subang Jaya 47500, Malaysia

Corresponding Author Email: ali.mohsen@uowa.edu.iq

https://doi.org/10.18280/ijht.420514

Received: 21 July 2024
Revised: 13 September 2024
Accepted: 27 September 2024
Available online: 31 October 2024

Keywords:
heat transfer, heat exchanger, pin fins, Nusselt number

ABSTRACT

In this paper, a study was performed for the effect of fins shape, spacing and arrangement on the inner pipe of a double pipe heat exchanger (DPHE). The DPHE models considered consist of concentric tubes with water and air as the hot and cold fluids in the inner and outer pipes, respectively. Computational fluid dynamics (CFD) simulation was incorporated to analyze the considered DPHE models with two different types of fins having the same surface area, cylindrical and conical pin fins. The distinction between cylindrical and conical pin fins is significant because their shapes influence the heat transfer and fluid flow characteristics within the heat exchanger. Therefore, understanding these differences is crucial for optimizing the design and performance of the double pipe heat exchanger. The numerical model was validated against experimental data from the available literature. Parameters such as fins spacing and arrangement were optimized to select the optimal configuration. The results showed that the cylindrical shaped pin fins are superior to the conical shaped fins although having the same overall surface area. The cylindrical and conical fins increased the airside Nusselt number by 20.22% and 13.95% compared to that of a smooth pipe DPHE, respectively. Additionally, increasing the fins spacing with a reduced number of fins decreased the airside Nusselt number but improved the overall performance of the DPHE by reducing the friction factor. Between 25 mm and 100 mm with increments of 25 mm, the fins spacing was optimized at 75 mm where the highest thermal performance factor was acquired. Finally, a staggered arrangement of the fins showed a negative impact on the hydrothermal performance of the DPHE as compared to an inline arrangement.

1. INTRODUCTION

A double pipe heat exchanger (DPHE) is a device that facilitates thermal energy transfer between two fluids via a solid surface [1-3]. It has been widely used in different industries including heating and cooling systems, power generation and pharmaceutical production [4-6]. The process of designing DPHE encompasses selecting suitable construction types, flow arrangements, tube and shell materials to fulfill predefined thermal energy transfer and pressure drop criteria [7-9].

Over the past few years, numerous investigations explored the impact of fin designs and arrangements on enhancing the thermal energy transfer. Jude et al. [10] conducted an extensive numerical investigation on a DPHE, comparing the numerical results with NTU method calculations. The study revealed a significant discrepancy between the numerical simulations and corresponding theoretical computations, with a notable 7.3% deviation between the two approaches. Kadhim et al. [11] studied the differences in thermal energy transfer in a cross-flow heat exchanger using ANSYS Fluent, demonstrating higher Nusselt number in finned tube heat exchangers compared to smooth tube counterparts. Similarly, Melvinraj et al. [12] numerically modeled ribbed tube heat exchangers, highlighting significant improvements in heat exchanger effectiveness through the use of ribbed tubes.

Sivalakshmi et al. [13] conducted experiments to evaluate the effectiveness of a DPHE with helical fins, demonstrating increased thermal performance with the use of fins. Balarama Kundu [14] performed experimental studies using longitudinal fins in shell and tube heat exchangers, indicating that trapezoidal fins led to higher Nusselt number and reduced pressure drops compared to rectangular fins.

Lee et al. [15] reported the effect of cribriform annular finned tubes on the thermal efficiency, revealing increased convective heat transfer coefficients with minor increases in pressure drop. Iqbal et al. [16] investigated optimal shapes for longitudinal triangular fins, demonstrating significant enhancements in the Nusselt number for various fin shapes. Furthermore, studies by Kanade et al. [17], Bhola et al. [18], and Sheikholeslami et al. [19] explored different aspects of heat exchanger design and performance, highlighting factors such as baffle geometry, tube inserts and flow characteristics. Córcoles et al. [20] and Ali and Jalal [21] conducted numerical

and experimental investigations, respectively, focusing on geometric factors and twisting configurations to enhance heat transfer efficiency. Finally, Fadaei et al. [22] and Huu-Quan et al. [23] investigated the performance enhancement in different heat exchanger configurations, emphasizing the impact of fluid properties and inner pipe geometry on heat transfer rates. Overall, these studies collectively contribute to a comprehensive understanding of heat exchanger performance and design optimization, offering valuable insights for future research and practical applications.

Based on the available literature and the relevant author informative insight and competence, no data was reported to study and compare the performance of DPHE using different fins of the same surface area. In this study, a numerical setup was introduced and three inner pipe configurations were considered and compared: smooth inner pipe, inner pipe with conical pin fins and inner pipe with cylindrical pin fins. Furthermore, the effects of other parameters such as fins spacing and arrangement on the hydrothermal performance of DPHEs were investigated.

2. HEAT EXCHANGER CONFIGURATIONS AND METHODOLOGY

In this section, the different investigated configurations of the DPHE are presented. The performance of these configurations is compared using CFD simulations, and the steps followed to accomplish the simulation cases are presented and explained in detail.

2.1 Heat exchanger configurations

The current study considers different configurations of single-phase DPHEs. Each configuration consists of two concentric cylinders with water in the inner tube and air in the outer shell. The dimensions of the DPHE are considered to be identical to those presented by Kumar et al. [24] for validation purpose. The length of both pipes is 1000 mm, while the outer pipe has inner and outer dimeters of 28.5 and 31.5 mm, respectively. The inner pipe has inner and outer dimeters of 9.5 and 11.5 mm, respectively. First, three cases are considered for the DPHE, i.e., smooth inner pipe, inner pipe with conical pin fins and inner pipe with cylindrical pin fins. Both conical and cylindrical pin fins have the same surface area. Figure 1 shows the three configurations of the DPHE. The first DPHE configuration acted as a reference case without fins, while 80 conical pin fins having a base diameter of 1.5 mm and a length of 5 mm were implemented on the outer surface of the inner pipe for the second configuration. Similarly, 80 cylindrical pin fins having a base diameter of 0.5585 mm and a similar length of 5 mm were implemented on the outer surface of the inner pipe for the third configuration. It should be noted that the base diameter of the cylindrical fins is taken as 0.5585 mm in order to have the same surface area as the conical fins. Both conical and cylindrical fins will have fin spacing of 50 mm along the pipe starting from the center of the pipe.

Additional four DPHE configuration were considered to study the effect of fins spacing. These models incorporated cylindrical pin fins with fins spacing of 25 mm, 50 mm, 75 mm and 100 mm that produce a number of fins of 156, 76, 52 and 36, respectively, as shown in Figure 2. For these models, cylindrical pin fins with a similar base diameter of 0.5585 mm and a height of 5 mm are implemented along the outer surface of the inner pipe.

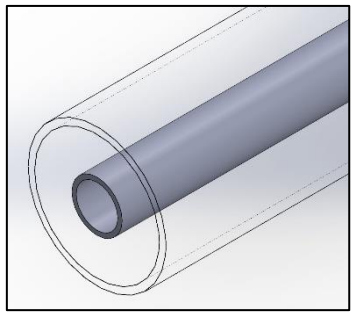

(a) Smooth inner pipe

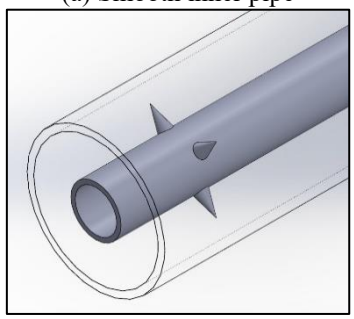

(b) Inner pipe with conical fins

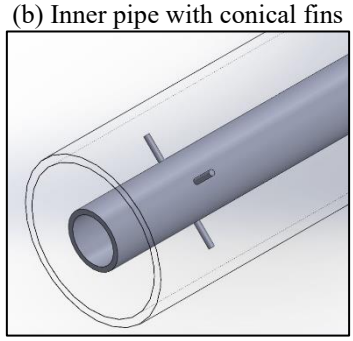

(c) Inner pipe with cylindrical fins

Figure 1. Three configurations of the DPHE with different inner pipe designs

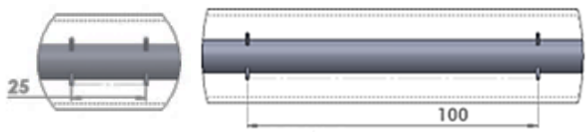

(a) 25 mm spacing (b) 100 mm spacing

Figure 2. Configurations of the DPHE with 25 mm and 100 mm fins spacing

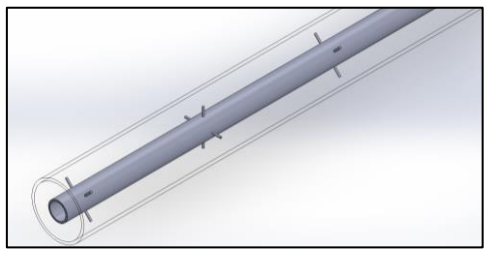

Figure 3. DPHE with staggered fins arrangement

Another geometrical parameter that incorporates staggered arrangement of cylindrical pin fins was investigated with fins spacing of 25 mm as shown in Figure 3. Similar number of

fins, fins dimensions and fins spacing were used with an inline arrangement case to enable a proper comparison for the effect of the fin's arrangement.

2.2 Governing equations

In this study, different assumptions were made to simplify the solution as follows:

(1) The working fluid is incompressible and Newtonian.
(2) Three-dimensional flow.
(3) Steady state flow.
(4) The flow is fully turbulent.

ANSYS Fluent CFD solver was used and the governing equations are expressed by the solver in the following forms [25]:

Conservation of mass:

$$\nabla.(\rho\vec{v}) = S_m \tag{1}$$

Conservation of momentum:

$$\nabla.(\rho\vec{v}\vec{v}) = -\nabla p + \nabla.(\bar{\bar{\tau}}) + \rho\vec{g} + \vec{F} \tag{2}$$

Conservation of energy:

$$\nabla.\left(\vec{v}(\rho E + P)\right) = -\nabla.\left(\sum_j h_j J_j\right) + S_h \tag{3}$$

For the turbulent flow, the realizable k-epsilon model was selected as it has a higher accuracy in simulating the behavior of the turbulent flow near the walls of heat exchangers with complex geometries while requiring smaller number of computational resources [26]. This model solves the following partial differential equations:

$$\frac{\partial}{\partial x_j}(\rho k u_j) = \frac{\partial}{\partial x_j}\left[(\mu + \frac{\mu_t}{\sigma_k})\frac{\partial k}{\partial x_j}\right] + G_k + G_b - \rho\varepsilon - Y_M + S_k \tag{4}$$

$$\frac{\partial}{\partial x_j}(\rho\varepsilon u_j) = \frac{\partial}{\partial x_j}\left[(\mu + \frac{\mu_t}{\sigma_\varepsilon})\frac{\partial \varepsilon}{\partial x_j}\right] + \rho C_1 S\varepsilon - \rho C_2 \frac{\varepsilon^2}{k + \sqrt{\nu\varepsilon}} C_{1\varepsilon}\frac{\varepsilon}{k} C_{3\varepsilon} G_b + S_\varepsilon \tag{5}$$

2.3 Materials and boundary conditions

Both pipes are considered to be made of copper with the thermal properties shown in Table 1. As for the working fluids, water is used as the hot fluid in the inner pipe while air is used as the cold fluid in the outer pipe with their thermal properties given in Table 2. No-slip boundary conditions were imposed on the walls of both the inner and outer pipes. Water is admitted at an inlet temperature of 293 K with a velocity corresponding to a Reynolds number of 2500, while air will be admitted at an inlet temperature of 323 K with four different velocities corresponding to Reynolds number values of 2500, 5000, 7500 and 10000. These values are based on the boundary conditions adopted by Kumar et al. [24]. The velocities were calculated based on the selected Reynolds number values using:

$$Re = \frac{\rho V D_H}{\mu} \tag{6}$$

Table 1. Thermal properties of copper

Property	Value
Density	8978 kg/m^3
Specific heat	381 J/kg·K
Thermal conductivity	387.6 W/m·K

Table 2. Thermal properties of air and water

Property	Value
Density (Air)	1.225 kg/m^3
Specific heat (Air)	1006.43 J/kg·K
Thermal conductivity (Air)	0.0242 W/m·K
Dynamic viscosity (Air)	1.7894×10^{-5} kg/m·s
Density (Water)	998.2 kg/m^3
Specific heat (Water)	4182 J/kg·K
Thermal conductivity (Water)	0.6 W/m·K
Dynamic viscosity (Water)	1.003×10^{-3} kg/m·s

2.4 Convergence criteria

To ensure that a converged solution is achieved, three methods were adopted to monitor convergence. The residuals for the continuity, momentum and energy equations were monitored and the solution was deemed converged when all residuals reached an accuracy of 10^{-5}. In addition, monitors were set for the temperature of the fluids exiting the heat exchanger to ensure that the most significant properties reached a steady state. In addition, the conservation of mass and energy were examined by checking the mass and energy imbalances which were shown to be very close to zero.

2.5 Calculation of the DPHE performance parameters

In the current study, heat is transferred from the hot fluid (water) in the inner pipe to the cold fluid (air) in the annulus region. The study aims to improve heat transfer characteristics along the DPHE, however, this could produce undesired effects such as an increase in the pressure drop caused by friction. Thus, parameters such as the friction factor and Nusselt number are calculated from the numerical data. The heat transfer rate for both fluids is obtained from [27]:

$$\dot{Q} = \dot{m} C_p (T_{out} - T_{in}) \tag{7}$$

Using the value from the above equation, the average value of heat coefficient is obtained by considering the contact surface area of the inner pipe and the difference between the average contact wall temperature of the inner pipe and the average temperature of the relevant fluid, as follows [27]:

$$h_{avg} = \frac{\dot{Q}}{A_s(T_{wall,avg} - T_{fluid,avg})} \tag{8}$$

Then, the Nusselt number is:

$$Nu = \frac{hd}{k} \tag{9}$$

The friction factor for both the cold fluids is determined based on Darcy-Weisbach equation [28] based on the average temperature of the relevant fluid, as follows:

$$\Delta p = f\frac{L}{d}\frac{\rho V^2}{2} \quad (10)$$

Lastly, the thermal performance factor is calculated using:

$$\eta_{fins} = \frac{\left(\frac{Nu_{fins}}{Nu_{smooth}}\right)}{\left(\frac{f_{fins}}{f_{smooth}}\right)^{\frac{1}{3}}} \quad (11)$$

2.6 Computational domains and meshing

The three-dimensional computational domains of the DPHE configurations were constructed using SolidWorks software. The designed parts were assembled then exported to ANSYS DesignModeler to define the different solid and fluid zones of each computational domain. Each domain consists of four zones, the outer pipe zone, inner pipe zone, hot fluid zone and cold fluid zone. As shown in Figure 4, the computational domains were meshed with unstructured tetrahedral cells, and inflation layers were added to the near-wall fluid regions around the inner pipe walls.

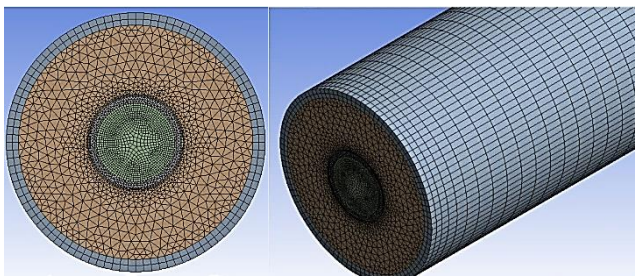

Figure 4. Mesh of the DPHE

Five different number of elements of 487336, 975483, 1267834, 1881703, and 2365149 were considered to acquire mesh. The Nusselt number value for air-side fluid was shown to be independent of the mesh size for number of elements of 1267834 and above as depicted in Figure 5.

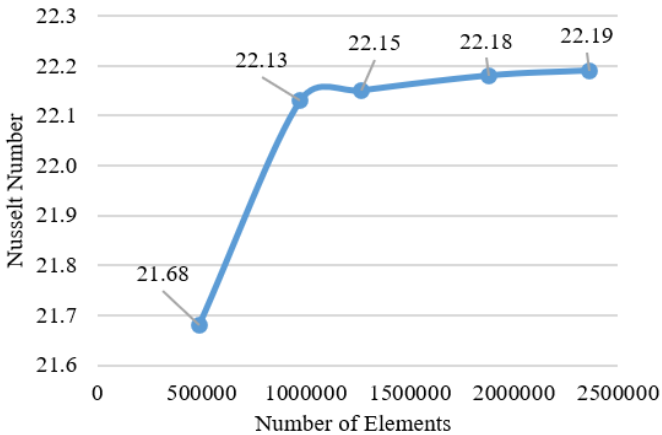

Figure 5. Nusselt number vs different mesh density

2.7 Validation of the simulation results

The results from the current study were validated by comparing the values of the airside Nusselt number with those reported by the experimental study of Kumar et al. [24]. Figure 6 presents the comparison between the Nusselt number values of the two studies at different Reynolds numbers. Both studies show similar trendlines with a very small difference in values. The simulated Nusselt number values obtained from this study have a mean deviation of 3.42% higher than the experimental values of Kumar et al. [24], with the highest deviation of 4.16% at an air Reynolds number of 7500 and lowest deviation of 2.63% at 5000 Reynolds number. Overall, the simulated Nusselt number results obtained in this study accord well with the experimental values. Thus, the current numerical simulation provides high accuracy results that can be used to conduct the study.

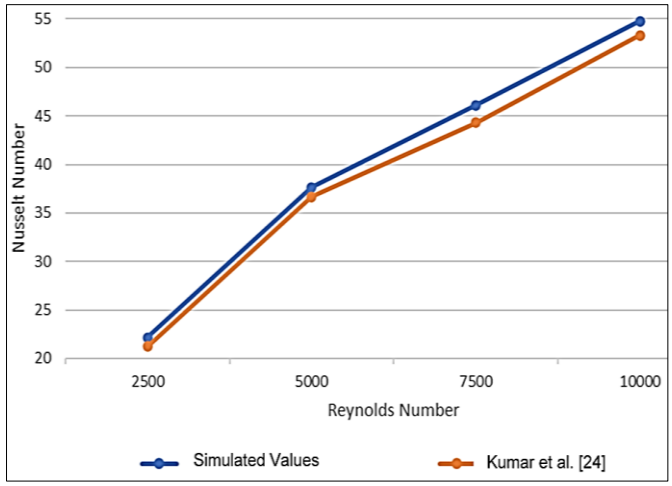

Figure 6. Comparison between the airside Nusselt number from the current study with Kumar et al. [24]

3. RESULTS AND DISCUSSION

3.1 Effect of inner pipe configuration

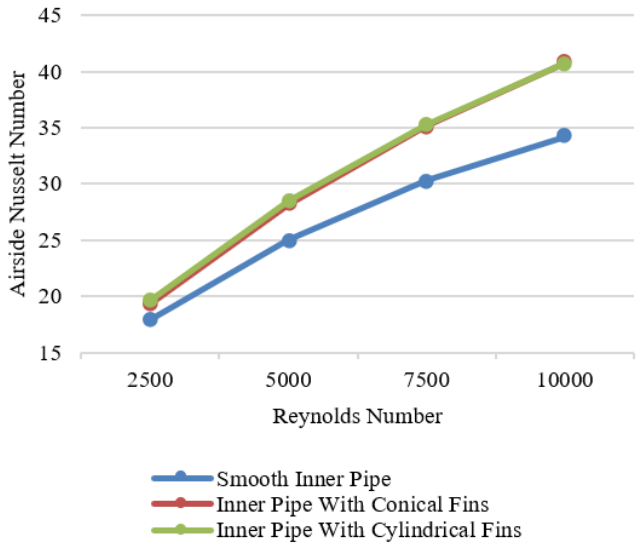

Figure 7. Airside Nusselt number for different inner pipe configurations

Figure 7 shows the airside Nusselt number for different inner pipe configurations. The airside Nusselt number increased as the Reynolds number increases across all three cases of different inner pipe configurations. This is attributed to the fact that at higher Reynolds numbers, the mass flow rate of the cold air is higher which enhances the airside heat

transfer rate. By further investigating Figure 7, we can see that the addition of cylindrical pin fins exhibits the highest increment in airside Nusselt number while the lowest values were observed with the smooth pipe case. When the cylindrical and conical pin fins are added, the mean airside Nusselt number increases by about 20.22 and 13.95%, respectively, compared to the smooth pipe case.

Figure 8 depicts the airside friction factor for the different inner pipe configurations. The friction factor seems to decrease with an increase in the airside Reynold number across all three cases. Generally, the addition of the pin fins significantly increases the airside friction factor, while the conical fins show higher values of the friction factor than the cylindrical fins. The implementation of the cylindrical and conical pin fins increased the mean friction factor by 27.88% and 34.7%, respectively, compared to the smooth pipe.

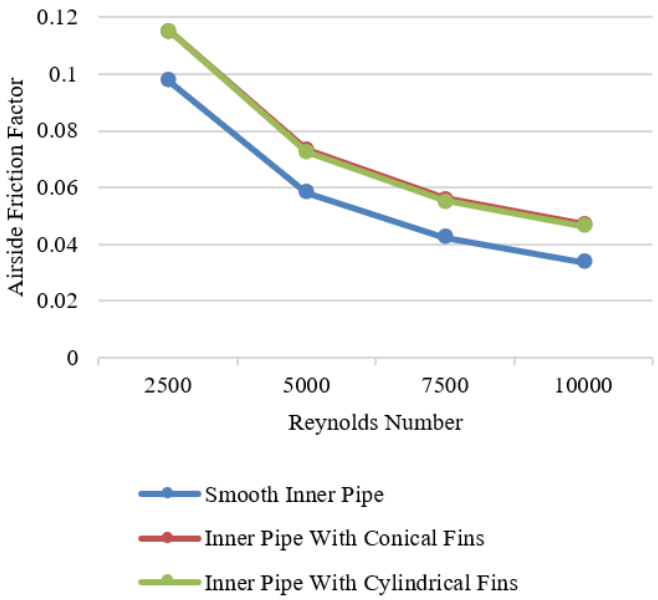

Figure 8. Airside friction factor for different inner pipe configurations

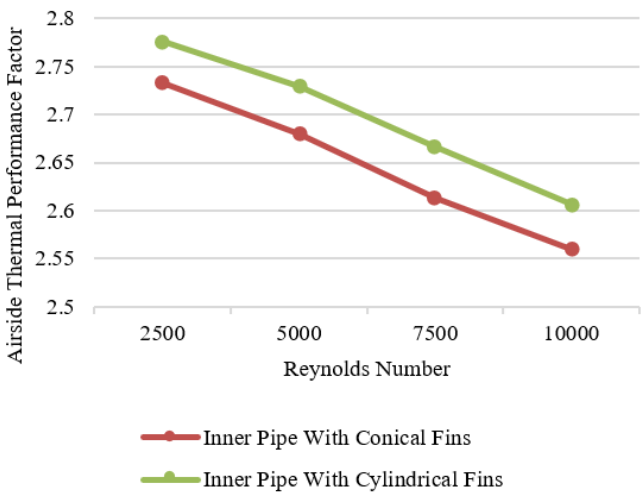

Figure 9. Airside thermal performance factor for different inner pipe configurations

Figure 9 shows the comparison of the airside thermal performance factor in the inner pipe with cylindrical and conical pin fins. The increase in the Reynolds number reduces the thermal performance factor for both cases. The DPHE with cylindrical pin fins show a superior thermal performance compared to the conical fins case. The cylindrical fins show a mean increase of 1.82% in the thermal performance factor compared to the conical fins.

From Figures 7, 8 and 9, the DPHE with cylindrical pin fins presents the best performance among the three investigated inner pipe configurations. The cylindrical fins increased the Nusselt number significantly with the lowest rise in the friction and thermal performance factors. So, the cylindrical pin fins will be adopted for the rest of the study to analyze the effects of the fins spacing and arrangement.

3.2 Effect of fins spacing

Figure 10 shows the effect of fins spacing on the airside Nusselt number. The values on the figure are at a Reynolds number of 2500. The increase in the fins spacing decreased the Nusselt number. This is caused by the reduction in both the surface area of heat transfer and flow turbulence when the fins spacing is increased, as the number of fins decreases. The implementation of cylindrical pin fins with fins spacing of 25 mm shows the highest airside Nusselt number of 21.38, with an increment of 14.67% as compared to the highest fins spacing of 100 mm.

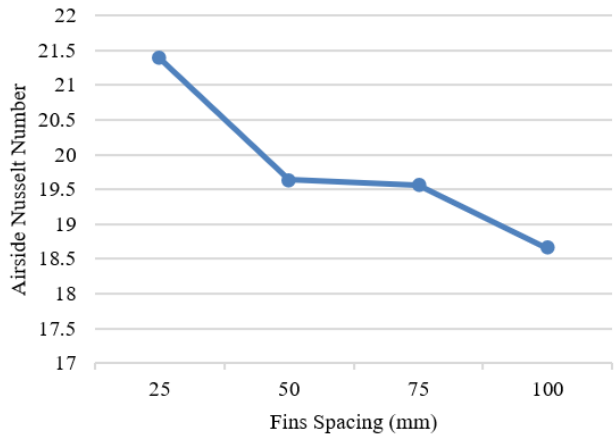

Figure 10. Airside Nusselt number for different fins spacing

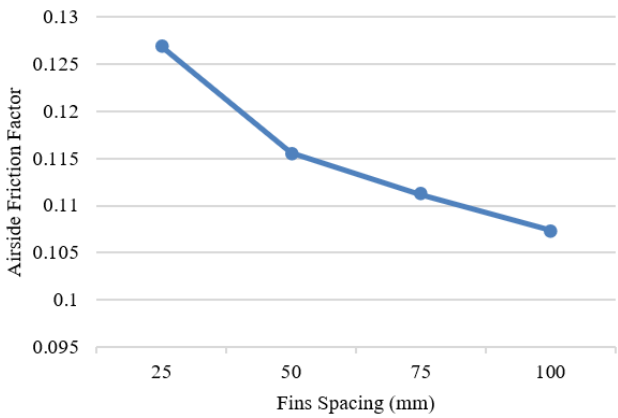

Figure 11. Airside friction factor for different fins spacing

The effect of the fins spacing on the airside friction factor is shown on Figure 11 at a Reynold number of 2500. The larger fins spacing produced a larger friction factor due to the increase in the number of fins. The reduction in the friction factor is by 18.12% when the fins spacing is increased from 25 to 100 mm.

Figure 12 shows the airside thermal performance factor for different fins spacing at 2500 Reynolds number. The highest performance of the DPHE is observed with fins spacing of 75 mm, which is 4.35% larger than the lowest thermal performance at 25 mm. This indicates that the implementation of cylindrical pin fins with fins spacing of 75 mm provides the best trade-off between heat transfer enhancement and pressure drop in the DPHE performance.

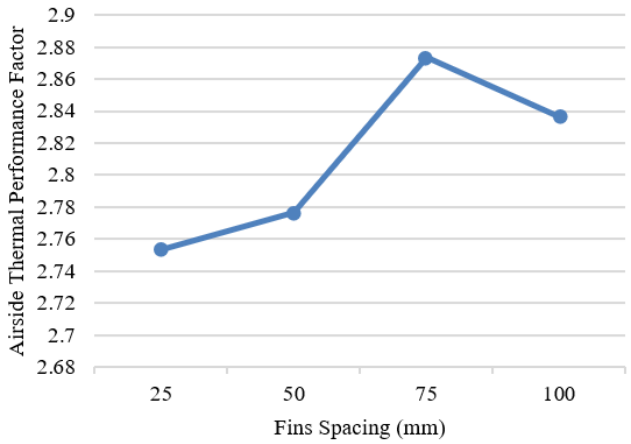

Figure 12. Airside thermal performance factor for different fins spacing

3.3 Effect of fins arrangement

The airside Nusselt number for two different fins arrangements at 2500 Reynolds number are presented on Figure 13. The implementation of inline fins arrangement seems to produce a higher value of the airside Nusselt number with an increment of 1.53% as compared to the staggered fins arrangement. So, the heat transfer process in the DPHE is more efficient with the consideration of inline fins arrangement.

Figure 14 depicts the influence of the pin fins arrangement of the airside friction factor. The inline arrangement produces a lower value of the friction factor by 1.16% as compared to the staggered fins arrangement. The staggered arrangement induces more disturbance in the flow path of the cold fluid, causing additional pressure drop in the airside region of the DPHE.

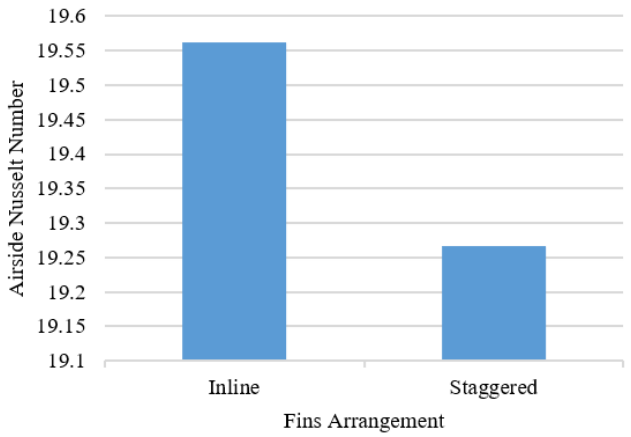

Figure 13. Airside Nusselt number for different fins arrangements

The airside thermal performance factor for the two different fins arrangements along the inner pipe of the DPHE are presented on Figure 15. The inline arrangement shows a superior performance due to the better thermal energy transfer and lower pressure drop. The thermal performance factor of the inline fins arrangement case is higher by 2.71% compared to the staggered arrangement case.

The consideration of the staggered fins arrangement on the inner pipe of the DPHE seems to have negative effects of the hydrothermal performance of the heat exchanger. It increases the pressure drop and produces a low Nusselt number as compared to the inline arrangement.

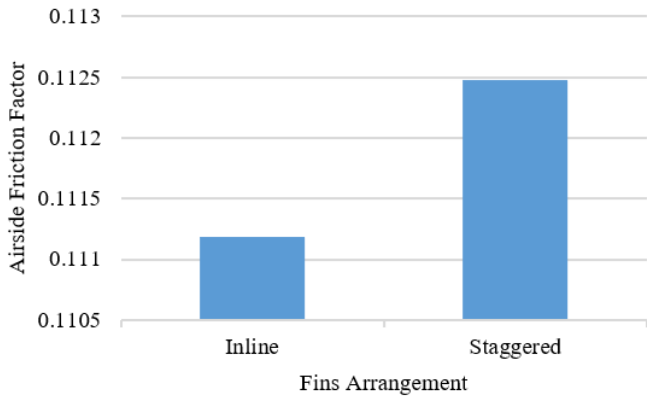

Figure 14. Airside friction factor for different fins arrangements

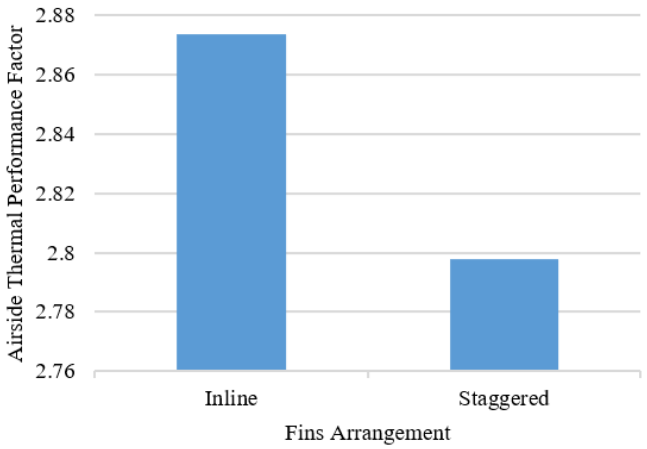

Figure 15. Airside thermal performance factor for different fins arrangements

4. CONCLUSIONS

In this study, different DPHE configurations were studied to analyze the effect of pin fins shape, spacing and arrangement on the hydrothermal performance of the system. Numerical methods were used to investigate the effects of each parameter by considering different models of the DPHE. The addition of pin fins improved the airside Nusselt number, while the cylindrical fins provided better improvement compared to the conical fins. However, the implementation of the pin fins introduced an increase in the pressure drop of the fluid that results from an increase in the friction factor. The fiction factor can be reduced by increasing the fins spacing and reducing the number of fins. This approach produces a lower Nusselt number as well, but the thermal performance factor increases which means that a better overall hydrothermal performance is acquired. Four fins spacings were considered

starting from 25 mm with increments of 25 mm, and the highest thermal performance factor was observed at the 75 mm fins spacing. An inline arrangement of the fins is recommended for the DPHE as it showed a better performance than the staggered arrangement.

Based on the findings of the current study, the authors recommend the following to be considered in future studies:

- The current study only investigates the implementation of conical and cylindrical pin fins with fin spacing of 25 mm, 50 mm, 75 mm and 100 mm. Further studies on different geometric design and considering a broader range of fin spacing can be conducted.
- The current study is solely based on CFD analysis. Further experimental studies can be conducted to complement the numerical results obtained.

REFERENCES

[1] Li, Z., Wei, L., Yang, T., Zhang, T., Li, R. (2024). Multi-objective optimization of the foam filled counterflow double-pipe heat exchanger under high temperature condition. International Journal of Heat and Mass Transfer, 223: 125230. https://doi.org/10.1016/j.ijheatmasstransfer.2024.125230

[2] Sheikhi Azizi, A., Jahanian, O., Mousavi Ajarostaghi, S.S., Arıcı, M. (2024). Employing uniform and non-uniform inner twisted elliptical tubes in a double-pipe heat exchanger. International Journal of Heat and Fluid Flow, 107: 109384. https://doi.org/10.1016/j.ijheatfluidflow.2024.109384

[3] Xiao, J., He, S., Xie, G., Wang, S., Zhang, Z. (2024). Visualization experiment and thermal-hydraulic behaviour of assembled self-rotating twisted tape in double-pipe heat exchangers. International Communications in Heat and Mass Transfer, 155: 107456. https://doi.org/10.1016/j.icheatmasstransfer.2024.107456

[4] Abed, A.M., Chauhan, B.S., Ayed, H., Mouldi, A., Ghoushchi, S.P., Deifalla, A., Mahariq, I. (2024). Heat transfer augmentation in a double pipe heat exchanger by tandem utilization of bubble injection and novel magnetic turbulators methods. Case Studies in Thermal Engineering, 57: 104298. https://doi.org/10.1016/j.csite.2024.104298

[5] Ashraf, G., Bilal, S., Ishaq, M., Khalid Saifullah, S., Alqahtani, A.S., Malik, M.Y. (2024). Thermodynamic optimization in laminar and fully developed flow in double pipe heat exchanger with arrow-shaped extended surfaces: A novel design. Case Studies in Thermal Engineering, 54: 103947. https://doi.org/10.1016/j.csite.2023.103947

[6] Luo, J., Asadollahzadeh, M., Chauhan, B.S., Abdalmonem, A., Elbadawy, I., Salah, B., Deifalla, A.F., Ghoushchi, S. P. (2024). First and second law analysis of a heat exchanger equipped with perforated wavy strip turbulator in the presence of water-CuO nanofluid. Case Studies in Thermal Engineering, 54: 103968. https://doi.org/10.1016/j.csite.2023.103968

[7] Ahirwar, B.K., Kumar, A. (2024). Experimental investigation for heat transfer performance of CuO-water nanofluid in a double pipe heat exchanger. Journal of Thermal Analysis and Calorimetry, 149(9): 4133-4151. https://doi.org/10.1007/s10973-024-12947-6

[8] Brown, C.S., Kolo, I., Banks, D., Falcone, G. (2024). Comparison of the thermal and hydraulic performance of single U-tube, double U-tube and coaxial medium-to-deep borehole heat exchangers. Geothermics, 117: 102888. https://doi.org/10.1016/j.geothermics.2023.102888

[9] Dhumal, G.S., Havaldar, S.N. (2023). Enhancing heat transfer performance in a double tube heat exchanger: Experimental study with twisted and helical tapes. Case Studies in Thermal Engineering, 51: 103613. https://doi.org/10.1016/j.csite.2023.103613

[10] Jude, G.D., Kumari, K.R., Maneiah, D. (2019). CFD analysis of double pipe parllel flow heat exchanger. International Journal of Innovative Technology and Research, 7(4): 9162-9166. https://core.ac.uk/download/pdf/228558454.pdf.

[11] Kadhim, Z.K., Kassim, M.S., Hassan, A.Y.A. (2016). CFD study for cross flow heat exchanger with integral finned tube. International Journal of Scientific and Research Publications, 6(6): 668.

[12] Melvinraj, C.R., Vishal V.C., Vicky, W., Thomas, J.T., Mithun, K., Simon, J.K. (2014). Comparative study of heat exchangers using CFD. International Journal of Engineering Research and Applications, 4(5): 118-120. https://www.ijera.com/papers/Vol4_issue5/Version%204/S04504118120.pdf.

[13] Sivalakshmi, S., Raja, M., Gowtham, G. (2021). Effect of helical fins on the performance of a double pipe heat exchanger. Materials Today Proceedings, 43: 1128-1131. https://doi.org/10.1016/j.matpr.2020.08.563

[14] Kundu, B. (2015). Beneficial design of unbaffled shell-and-tube heat exchangers for attachment of longitudinal fins with trapezoidal profile. Case Studies in Thermal Engineering, 5: 104-112. https://doi.org/10.1016/j.csite.2015.03.001

[15] Lee, D.H., Jung, J.M., Ha, J.H., Cho, Y.I. (2012). Improvement of heat transfer with perforated circular holes in finned tubes of air-cooled heat exchanger. International Communications in Heat and Mass Transfer, 39(2): 161-166. https://doi.org/10.1016/j.icheatmasstransfer.2011.11.009

[16] Iqbal, Z., Syed, K.S., Ishaq, M. (2013). Optimal fin shape in finned double pipe with fully developed laminar flow. Applied Thermal Engineering, 51(1-2): 1202-1223. https://doi.org/10.1016/j.applthermaleng.2012.10.036

[17] Kanade, R.H., Kailash, B.A., Gowreesh. (2015). Heat transfer enhancement in a double pipe heat exchanger using CFD. International Research Journal of Engineering and Technology (IRJET), 2(9): 419-430. https://www.irjet.net/archives/V2/i9/IRJET-V2I968.pdf.

[18] Bhola, M., Kumar, M.V., Singh, D.S. (2015). Heat transfer enhancement in concentric tube heat exchanger in ANSYS FLUENT 14.5. IJISET-International Journal of Innovative Science, Engineering & Technology, 2(3): 375-379. https://ijiset.com/vol2/v2s3/IJISET_V2_I3_59.pdf.

[19] Sheikholeslami, M., Hatami, M., Jafaryar, M., Farkhadnia, F., Ganji, D.D., Gorji-Bandpy, M. (2015). Thermal management of double-pipe air to water heat exchanger. Energy Buildings, 88: 361-366. https://doi.org/10.1016/j.enbuild.2014.11.076

[20] Córcoles, J.I., Moya-Rico, J.D., Molina, A.E., Almendros-Ibáñez, J.A. (2020). Numerical and experimental study of the heat transfer process in a double pipe heat exchanger with inner corrugated tubes. International Journal of Thermal Sciences, 158: 106526. https://doi.org/10.1016/j.ijthermalsci.2020.106526
[21] Ali, M.H., Jalal, R.E. (2021). Experimental investigation of heat transfer enhancement in a double pipe heat exchanger with a twisted inner pipe. Heat Transfer, 50(8): 8121-8133. https://doi.org/10.1002/htj.22269
[22] Fadaei, M., Izadi, M., Assareh, E., Ershadi, A. (2023). Conjugated non-Newtonian phase change process in a shell and tube heat exchanger: A parametric-geometric analysis. Applied Thermal Engineering, 220: 119795. https://doi.org/10.1016/j.applthermaleng.2022.119795
[23] Huu-Quan, D., Mohammad Rostami, A., Shokri Rad, M., Izadi, M., Hajjar, A., Xiong, Q. (2021). 3D numerical investigation of turbulent forced convection in a double-pipe heat exchanger with flat inner pipe. Applied Thermal Engineering, 182: 116106. https://doi.org/10.1016/j.applthermaleng.2020.116106
[24] Kumar, S., Dinesha, P., Sai Krishna, K.R.N. (2019). Experimental and numerical analysis of cylindrical turbulators in a double pipe heat exchanger under turbulent flow conditions. Journal of Turbulence, 20(4): 245-262. https://doi.org/10.1080/14685248.2019.1623405
[25] Tukkee, A.M., Al-Kayiem, H.H., Gilani, S.I.U. (2023). Effect of density variation method and air humidity consideration on the computational simulation of solar vortex power generation systems. Thermal Science and Engineering Progress, 37: 101574. https://doi.org/10.1016/j.tsep.2022.101574
[26] Shaheed, R., Mohammadian, A., Kheirkhah Gildeh, H. (2019). A comparison of standard k-ε and realizable k-ε turbulence models in curved and confluent channels. Environmental Fluid Mechanics, 19(2): 543-568. https://doi.org/10.1007/s10652-018-9637-1
[27] Oleiwi, A., Mohsen, A.M., Abdulkadhim, A., Abed, A.M., Laidoudi, H., Abderrahmane, A. (2023). Experimental and numerical study on the heat transfer enhancement over scalene and curved-side triangular ribs. Heat Transfer, 52(5): 3433-3452. https://doi.org/10.1002/htj.22835
[28] Afzal, N. (2007). Friction factor directly from transitional roughness in a turbulent pipe flow. Journal of Fluids Engineering, 129(10): 1255-1267. https://doi.org/10.1115/1.2776961

NOMENCLATURE

A_s	Surface area, m^2
C_1	Variable
C_2, $C_{1\varepsilon}$	Constants
$C_{3\varepsilon}$	Buoyancy effect on the dissipation rate
C_p	Specific heat, J/kg·K
d	Diameter, m
D_H	Hydraulic diameter, m
E	Energy, J
f	Friction factor
$\vec{F}$	Forces
g	Acceleration of gravity, m/s^2
G_k, G_b	Turbulence kinetic energy generation terms
h	Enthalpy, J - Convection heat transfer coefficient, W/m^2·K
J	Species
k	Turbulence kinetic energy, m^2/s^2
L	Length, m
$\dot{m}$	mass flowrate, kg/s
Nu	Nusselt number
p	Pressure, Pa
$\dot{Q}$	Heat transfer rate, W
Re	Reynolds number
S	Modulus of the strain tensor
S_m, S_h, S_k, S_ε	Source terms
T	Temperature, K
V	Velocity, m/s
$\vec{v}$	Velocity vector, m/s
Y_M	Contribution to the overall dissipation rate

Greek symbols

ε	Kinetic energy dissipation rate, m^2/s^3
η	Thermal performance factor
μ	Viscosity, N.s/m^2
μ_t	Turbulent viscosity, m^2/s
ν	Kinematic viscosity, m^2/s
ρ	Density, kg/m^3
σ_k, σ_ε	Turbulent Prandtl numbers
$\bar{\bar{\tau}}$	Stress tensor, N/m^2